Magnetoelectronic properties of chiral carbon nanotubes and tori

To cite this article: F L Shyu *et al* 2006 *J. Phys.: Condens. Matter* **18** 8313

View the article online for updates and enhancements.

Magnetoelectronic properties of chiral carbon nanotubes and tori

F L Shyu[1], C C Tsai[2], C H Lee[2] and M F Lin[2]

[1] Department of Physics, Chinese Military Academy, Kaohsiung, Taiwan 830, Republic of China
[2] Department of Physics, National Cheng Kung University, Tainan, Taiwan 701, Republic of China

E-mail: fl.shyu@msa.hinet.net

Abstract

Magnetoelectronic properties of chiral carbon nanotubes and toroids are studied for any magnetic field. They are sensitive to the changes in the magnitude and the direction of the magnetic field, as well as the chirality. The important differences between chiral and achiral carbon nanotubes include band symmetry, band curvature, band crossing, band-edge state, state degeneracy, band spacing, energy gap, and semiconductor–metal transition. Carbon tori also exhibit the strong chirality dependence on the field modulation of discrete states. Chiral carbon tori might differ from chiral carbon nanotubes in energy-gap modulation, density of states, and state degeneracy.

1. Introduction

Since carbon nanotubes (CNTs) were discovered in 1991 by Iijima [1], the great potential for novel nano-devices has motivated a lot of studies [2–26]. A single-walled carbon nanotube could be considered as a rolled-up graphite sheet. Its structure is thus fully specified by the transverse and the longitudinal lattice vectors $\mathbf{R_x} = m\mathbf{a_1} + n\mathbf{a_2}$ and $\mathbf{R_y} = p\mathbf{a_1} + q\mathbf{a_2}$, where $\mathbf{a_1}$ and $\mathbf{a_2}$ are the primitive lattice vectors of a graphite sheet (details in [4]). The radius and the chiral angle of a (m, n) carbon nanotube are, respectively, $r = |\mathbf{R_x}|/2\pi = b\sqrt{3(m^2 + mn + n^2)}/2\pi$ and $\theta = \tan^{-1}\frac{-\sqrt{3}n}{(2m+n)}$. $b = 1.42$ Å is the C–C bond length. $N_u = 4\sqrt{(m^2 + mn + n^2)(p^2 + pq + q^2)/3}$ is the number of carbon atoms in a primitive unit cell. The radius is between 3 and 100 Å, and its length can reach several micrometres.

A carbon nanotube is either metallic or semiconducting, which is mainly determined by its radius and chirality [2–18]. When the curvature effects due to the misorientation of $2p_z$ orbitals are taken into account, there are three types of carbon nanotubes: (I) a gapless metal for $m = n$; (II) a narrow-gap semiconductor for $2m + n = 3I$ (where I is an integer and $m \neq n$); and (III) a moderate-gap semiconductor for others. For type-II and type-III CNTs, their energy gaps

are, respectively, proportional to $1/r^2$ and $1/r$. The dependence of energy gap on radius and chirality has also been verified by scanning tunnelling microscopy (STM) [19, 20]. Specifically, the current–voltage (I–V) curves can distinguish metallic CNTs from semiconducting CNTs. Furthermore, the differential conductance (dI/dV) is deduced to be proportional to the density of states (DOS). The dI/dV–V curves show a number of peak structures due to the van Hove singularities (vHs) of the one-dimensional DOS. Each prominent peak corresponds to the band-edge state of the parabolic band. The energy difference between two prominent peaks is the band spacing. Metallic CNTs have a finite conductance at the Fermi energy (E_F), whereas semiconducting CNTs have a vanishing conductance. As for the energy gap E_g, this is the energy spacing between two prominent peaks nearest to E_F. The small band gaps and their $1/r^2$ dependence of type-II CNTs are further verified by low-temperature scanning tunnelling microscopy [21] and transport measurements [22].

The electronic structures of CNTs in the presence of a magnetic field have been studied within the effective-mass approximation [6] and the tight-binding model [10–16]. The magnetic field could induce drastic changes in the energy dispersion and energy gap. Furthermore, electronic properties exhibit periodical Aharonov–Bohm (AB) oscillations with a period of $\phi_0 = hc/e$ (the fundamental magnetic flux), if the magnetic field is parallel to the tube axis and the Zeeman splitting is neglected. Experimentally, the AB effect on CNTs has been identified by measurements on transport properties [23–26]. In addition to the parallel magnetic field, the band structures of achiral CNTs have also been investigated theoretically for any magnetic field [6, 10–18]. The direction of the magnetic field significantly affects the electronic properties, such as energy dispersion, state degeneracy, and energy gaps.

The two ends of CNTs may be able to knit together seamlessly [27, 28]. Carbon atoms can form a carbon toroid (CT). A CT is a thin system, since its radius (R) is much larger than its height ($2r$) or width [29–33]. The electronic properties are dominated by the toroid geometry, such as the radius, height, and chiral angle [34–42]. According to the energy gap, there are four types of CTs [39]: (I) $E_g \sim 0$ (armchair CTs); (II) $E_g \propto 1/r^2$; (III) $E_g \propto 1/r$; and (IV) $E_g \propto 1/R$ (armchair CTs). Both CTs and CNTs have cylindrical symmetry. When a magnetic field parallel to the toroid axis is applied, CTs could exhibit periodic AB oscillations in the absence of the Zeeman splitting, as seen in CNTs. The electronic structures of achiral CTs were studied for any magnetic field [38–42]. They strongly depend on the direction and the magnitude of the magnetic field. All of the above-mentioned studies of magnetoelectronic properties are mainly focused on achiral carbon nanotubes (ACNTs) and achiral carbon toroids (ACTs). It is worth studying the dependence of magnetoelectronic properties on the chiral angle.

In this work, we mainly study magnetoelectronic properties of chiral carbon nanotubes (CCNTs) and chiral carbon toroids (CCTs) using the tight-binding model for any magnetic field. The curvature effect and the Zeeman splitting are included in the calculations. The state energy, density of states, and energy gaps are discussed. Our study shows that magnetoelectronic states are very sensitive to changes in the magnetic field and the chirality. The magnetic field could induce a shift and a coupling of subbands. Such effects depend on chirality, and so do the magnetoelectronic properties (band symmetry, band curvature, band crossing, band-edge state, state degeneracy, band spacing, and energy gap).

2. Theory

The π-electron states of a CNT are calculated within the tight-binding model, as is done for a graphite sheet. The curvature effect and the periodical boundary condition are taken into account simultaneously. For the π-band structure of a graphite sheet, the Hamiltonian in the

subspace built from the two tight-binding functions $\Phi^A(k_x, k_y)$ and $\Phi^B(k_x, k_y)$ is a 2×2 Hermitian matrix,

$$H = \begin{pmatrix} 0 & H_{12}(k_x, k_y) \\ H_{12}^*(k_x, k_y) & 0 \end{pmatrix}, \tag{1}$$

where $H_{12}(k_x, k_y) = -\Sigma_{i=1}^3 \gamma_i \exp(-i\mathbf{k} \cdot \mathbf{r}_i)$. The Hamiltonian matrix elements include three nearest-neighbour interactions. $\mathbf{k}$ is the Bloch wavevector, and $\mathbf{r}_i$ is the relative vector of the two neighbouring atoms (A atom and B atom). As a result of the misorientation of $2p_z$ orbitals on the nanotube surface, the hopping integrals along the different directions are, respectively, given by $\gamma_1 = \gamma_0[1 - b^2 \sin^2 \theta / 8r^2]$, $\gamma_2 = \gamma_0[1 - b^2(\sin \theta + \sqrt{3} \cos \theta)^2 / 32r^2]$, and $\gamma_3 = \gamma_0[1 - b^2(\sin \theta - \sqrt{3} \cos \theta)^2 / 32r^2]$ [8]. γ_0 ($\sim 2.6 - 3$ eV) [4–18] is the hopping integral of a graphite sheet. The electronic states of a CNT are characterized by the discrete quantum number (subband) J ($= 1, 2, \ldots, N_u/2$) and the longitudinal wavevector k_y ($-\pi \leqslant k_y R_y \leqslant \pi$). J comes from the transverse boundary condition. The maximum subband index $J_{\max}$ depends on the number of atoms in a primitive unit cell (or radius and chiral angle). The similar quantum numbers could also be found in quantum rings. $R_y = |\mathbf{R_y}| = b\sqrt{3(p^2 + pq + q^2)}$ is the periodic distance along the nanotube axis.

CNTs are in the presence of a uniform magnetic field. The angle between $\mathbf{B}$ and the nanotube axis is α; that is, $\mathbf{B} = B \cos \alpha \hat{y} + B \sin \alpha \hat{x} = B_\parallel \hat{y} + B_\perp \hat{x}$. $B_\parallel$ induces the shift $J \rightarrow J + \phi \cos \alpha / \phi_0$, and $B_\perp$ leads to the coupling of different Js. $\phi = \pi r^2 B$ is the applied magnetic flux. The vector potential corresponding to $\mathbf{B}$ is chosen as $\mathbf{A} = rB \cos \alpha/2\hat{x} + rB \sin \alpha \sin(x/r)\hat{y}$. The vector potential causes the Peierls phase $G = \int \mathbf{A} \cdot d\mathbf{D}$ in the tight-binding function. This phase would make the subbands mix with one another; therefore, the Hamiltonian is characterized by an $N_u \times N_u$ Hermitian matrix. The matrix element associated with the k_x state of the A site and the k_x' state of the B site is given by [16]

$$\langle \Phi_{k_x'}^B | H | \Phi_{k_x}^A \rangle = \frac{-2}{N_u} \sum_{R^A} \sum_{R^B} \gamma_i e^{-i\Delta k_x x} e^{-i(k_x' + \phi \cos \alpha/\phi_0 r)\Delta x} e^{-ik_y \Delta y} e^{i\frac{e}{\hbar}\Delta G}, \tag{2}$$

where the phase difference due to $\mathbf{A}$ is

$$\Delta G = G_{R^A} - G_{R^B} = \begin{cases} r^2 B \sin \alpha \dfrac{\Delta y}{\Delta x} \left[\cos \dfrac{x}{r} - \cos \dfrac{(x + \Delta x)}{r} \right] & \Delta x \neq 0, \\ rB \sin \alpha \Delta y \sin \dfrac{x}{r} & \Delta x = 0. \end{cases} \tag{3}$$

$\mathbf{R}^A = (x, y)$, $\mathbf{R}^B = (x', y')$, and $\Delta \mathbf{R} = \mathbf{R}^B - \mathbf{R}^A = (\Delta x, \Delta y)$.

The electronic states of a CNT are obtained by diagonalizing the $N_u \times N_u$ Hamiltonian matrix. The state energy is $E^h(J, k_y, \phi, \alpha)$, where $h = v$ (c) represents the π (π^*) state with negative (positive) energy. The Zeeman splitting energy is $E_z = g\sigma\phi/m^* r^2 \phi_0$. $g \approx 2$ is the same as that of the pure graphite. $\sigma = \pm 1/2$ is the electron spin and m^* is the bare electron mass. The total energy is $E^h(J, k_y, \phi, \alpha; \sigma) = E^h(J, k_y, \phi, \alpha) + E_z$. The density of states is useful in understanding the low-frequency electronic structures. It is defined as

$$D(\omega, \phi, \alpha) = 2 \sum_{J,h=c,v} \int_{1stBZ} \frac{dk_y}{2\pi} \frac{\Gamma}{\pi} \frac{1}{[\omega - E^h(J, k_y, \phi; \alpha)]^2 + \Gamma^2}. \tag{4}$$

$\Gamma = 5 \times 10^{-5} \gamma_0$ is the broadening parameter.

As for a carbon toroid, its geometric structure is formed by knitting seamlessly the two ends of a CNT together. $R = |\mathbf{R_y}|/2\pi = b\sqrt{3(p^2 + pq + q^2)}/2\pi$ is the radius of a CT. $2r$, twice the radius of a CNT, represents the height of a CT. The additional boundary condition along the nanotube axis would introduce the longitudinal discrete quantum number L ($= k_y R$). $L = 1, 2, \ldots, N_v$, and N_v is the greatest common divisor of (p, q). The geometric structure is

defined by the parameters (m, n, p, q), and each electronic state is characterized by (J, L). J_{max} depends on the toroid height and the chiral angle, while L_{max} is determined by the toroid radius. J and L could serve as good quantum numbers for the electronic states; furthermore, they need to satisfy conservation laws in optical excitations and inelastic Coulomb scatterings. When a CT exists in an electromagnetic (EM) field with an electric polarization parallel (perpendicular) to the symmetric axis, the optical selection rule is $\Delta J = \pm 1$ and $\Delta L = 0$ ($\Delta J = 0$ and $\Delta L = \pm 1$) [43]. As to the Coulomb excitations in a CT, the transfer of the transverse quantum number J is conserved in the electron–electron interactions [44]. When a carbon toroid is in a uniform magnetic field, there is an angle (α) between **B** and the toroid axis. The effect of the magnetic field on J is negligible, mainly owing to the large energy spacing between states with different Js. Moreover, the perpendicular component of **B** would couple the different Ls. The calculations on the magneto-band structure of a CT are similar to those of a CNT. The details could be found in [41]. The DOS of a CT is calculated by replacing the integration of the wavevector k_y in equation (4) with the summation of the discrete quantum number L.

3. Results and discussion

Type-II CCNTs, including the (18,6) CNT ($\theta = -13.9°$, $r = 8.5$ Å) and the (18,12) CNT ($\theta = -23.4°$, $r = 10.24$ Å), are first chosen as a model study. The low-energy magneto-band structures are shown in figures 1(a) and (b). At $\phi = 0$, the two conduction or valence bands nearest to the Fermi level ($E_F = 0$) are characterized by the subbands J_l and $N_u/2 - J_l$ (the solid curves). The band-edge states are located at the nonzero wavevector $k_y^{ed} \neq 0$. They correspond, respectively, to the (J_l, k_y^{ed}) and $(N_u/2 - J_l, -k_y^{ed})$ states. The energy dispersions are parabolic near the band-edge states, but linear away from them. Each band is asymmetric about $k_y = 0$; that is, $E^{c,v}(J_l, k_y) \neq E^{c,v}(J_l, -k_y)$. The two bands intersect each other at $k_y = 0$, and their electronic states are doubly degenerate ($E^{c,v}(J_l, k_y) = E^{c,v}(N_u/2 - J_l, -k_y)$). The whole electronic structure is symmetric about $k_y = 0$. Furthermore, there is no band spacing between two band-edge states.

A parallel magnetic field strongly affects the subbands, and its effects on the (J_l, k_y) and $(N_u/2 - J_l, -k_y)$ states are different. As a result, it would drastically change the electroinc structure. The energy dispersions are parabolic even away from the band-edge states, and their curvatures become small. The band symmetry about $k_y = 0$ is destroyed, and the double degeneracy is absent. The energy bands could no longer intersect at $k_y = 0$. The band-edge states exhibit a large shift, and there exists an obvious band spacing between them. Moreover, the energy gap is greatly widened. When the magnetic field gradually deviates from the nanotube axis, the effects of **B** on the band structure are getting weak. The band spacing increases as α grows from $0°$. Then it would decrease with a further increase in α. However, the opposite is true for the band curvature. At large α, the energp gap, the band spacing, and the shift of the band-edge states are relatively small. For the perpendicular magnetic field, the crossing point of the energy bands at $k_y = 0$, the vanishing band spacing, the band symmetry, and the double degeneracy are recovered to the case of $\phi = 0$. Also note that the energy gap, band spacing, band-edge states, and band curvature strongly depend on the chiral angle. The energy gap and band spacing are comparatively large for CCNTs with small chiral angles.

Regarding type-III CCNTs, we select the (16, 2) CNT ($\theta = -5.8°$, $r = 6.7$ Å) and the (16, 8) CNT ($\theta = -19.1°$, $r = 8.3$ Å). The magnetoelectronic structures are shown in figures 1(c) and (d), respectively. They display the change of band curvature, the shift of band-edge states, the asymmetric band structure about $k_y = 0$ at $\alpha \neq 90°$, and the destruction of the double degeneracy at $\alpha \neq 90°$. There exist certain important differences between type-III
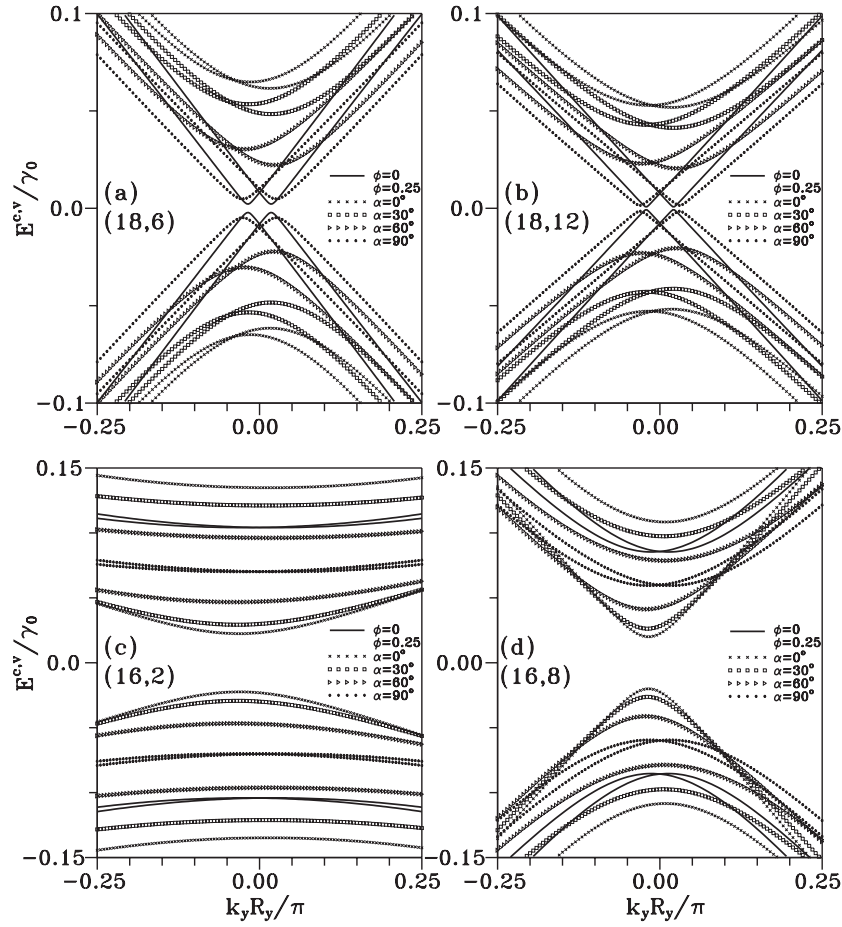
Figure 1. The low-energy magnetoelectronic structures for the (a) (18, 6), (b) (18, 12), (c) (16, 2), and (d) (16, 8) CCNTs at $\phi = 0$; $\phi = 0.25\phi_0$ and different field directions.

CCNTs and type-II CCNTs. As to the former: (I) band crossing is absent except at $\alpha = 90°$ or $\phi = 0$; (II) the shift in the wavevector of the band-edge state is less apparent; (III) the band spacing exhibits a stronger ϕ-dependence; (IV) the energy gap is relatively large; and (V) the energy gap grows with increasing α.

It is worth making a detailed comparison of the magnetoelectronic structures between chiral CNTs and achiral CNTs (e.g. type-I (10, 10), type-II (18, 0) and type-III (17, 0) CNTs in [16]). As for achiral CNTs, each energy band is symmetric about $k_y = 0$, i.e. $E^{c,v}(J, k_y) = E^{c,v}(J, -k_y)$. The band symmetry remains unchanged even in the presence of the magnetic field. The band crossing is absent for the low-energy bands. The double degeneracy arises from $E^{c,v}(J_l, k_y) = E^{c,v}(N_u/2 - J_l, k_y)$ and $E^{c,v}(J_l, k_y) = E^{c,v}(J_l, -k_y)$ for zizag CNTs and armchair CNTs, respectively. The magnetic field does not destroy the double degeneracy of armchair CNTs. The band-edge states of zigzag CNTs always stays at $k_y^{\text{ed}} = 0$. Moreover, those of armchair CNTs have no band spacing. The above-mentioned important differences further illustrate that chirality plays an important role in magnetoelectronic structures.

The density of states reveals the main features of magneto-band structures, such as the energy dispersion, state degeneracy, and band spacing. It is associated with the number of
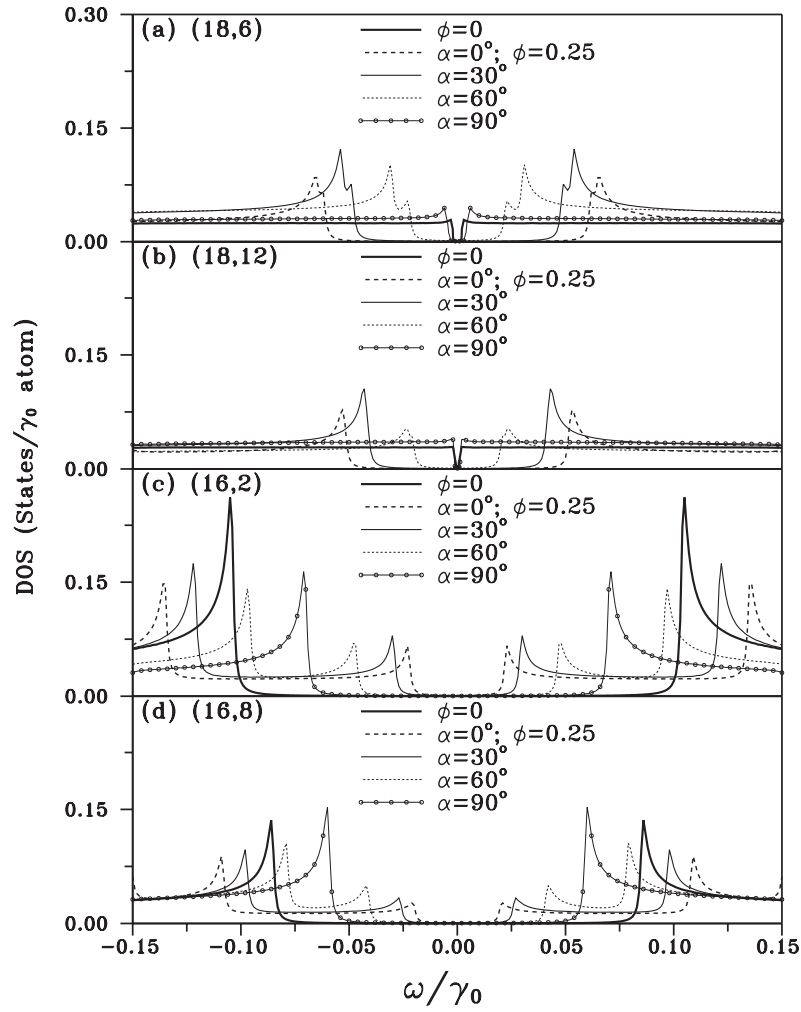
Figure 2. Density of states for the (a) (18, 6), (b) (18, 12), (c) (16, 2), and (d) (16, 8) CCNTs at $\phi = 0$; $\phi = 0.25\phi_0$ and different field directions.

excitation channels and is useful in explaining the optical absorption spectra. The DOS of type-II CCNTs is shown in figures 2(a) and (b). It could exhibit the asymmetric square-root divergent peaks. Each peak comes from the band-edge state of a parabolic energy dispersion. The energy difference between two neighbouring peaks is the band spacing. The peak height is determined mainly by the inverse of the band curvature and the state degeneracy. The magnetic field at $\alpha \neq 90°$ could destroy the double degeneracy and thus induce a pair of peak structures. Such peaks depend on the chiral angle, and the direction and the magnitude of the magnetic field. It is relativley easy to observe them in CNTs with small chiral angles (figure 2(a)). A pair of peaks would gradually approach the Fermi level for an increase in α. Their energy difference would grow and then decline. However, at $\alpha = 90°$ or $\phi = 0$, there only exists a single weak peak near the right-hand (left-hand) neighbourhood of $E_F = 0$. There are three main differences between type-III CCNTs and type-II CCNTs in DOS. The former, as shown in figures 2(c) and (d), exhibit relativley prominent peaks. A pair of peak structures is very clear;
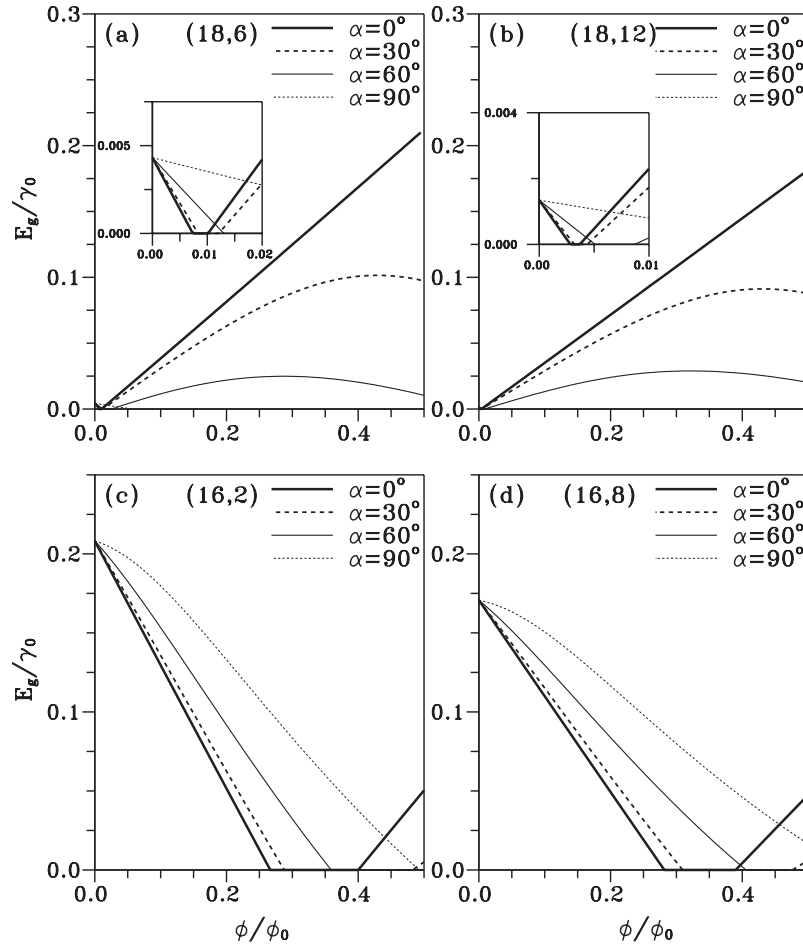
Figure 3. Flux-dependent energy gaps at different αs for the (a) (18, 6), (b) (18, 12), (c) (16, 2), and (d) (16, 8) CCNTs. The insets show details of the semiconductor–metal transitions.

that is, their energy difference is much larger than that of the latter. The two peaks are close to each other as α increases. The predicted DOS could be test by STM, transport measurements, and absorption spectroscopy.

Quantum effects induced by a magnetic field could effectively modulate the energy gaps of CNTs. Figures 3(a) and (b) present the magnetic-flux-dependent energy gap of type-II CCNTs at $\phi \leqslant 0.5\phi_0$ and different αs. The Zeeman splitting, which would reduce the energy gap by twice $|E_z|$, is included in the calculations. At $\phi = 0$, the curvature effect induces a small energy gap. E_g decreases as ϕ gradually grows. The energy gap would change from a finite value to zero at a specific magnetic flux ϕ_{SMT} (the insets in figures 3(a) and (b)). The parabolic valence (spin-up) and conduction (spin-down) bands just intersect at $E_F = 0$, so the semiconductor–metal transition (SMT) (or the complete energy-gap modulation) occurs at ϕ_{SMT}. These two energy bands would overlap and then separate from each other on a further increase in ϕ. As a result, there are twice the SMTs except at $\alpha = 90°$. The Zeeman splitting would metallize CNTs at $\phi \geqslant \phi_{SMT}$ and $\alpha = 90°$, since its energy is in excess of the energy gap due to the perpendicular magnetic field. At small α, the variation of E_g with ϕ is relatively quick, and
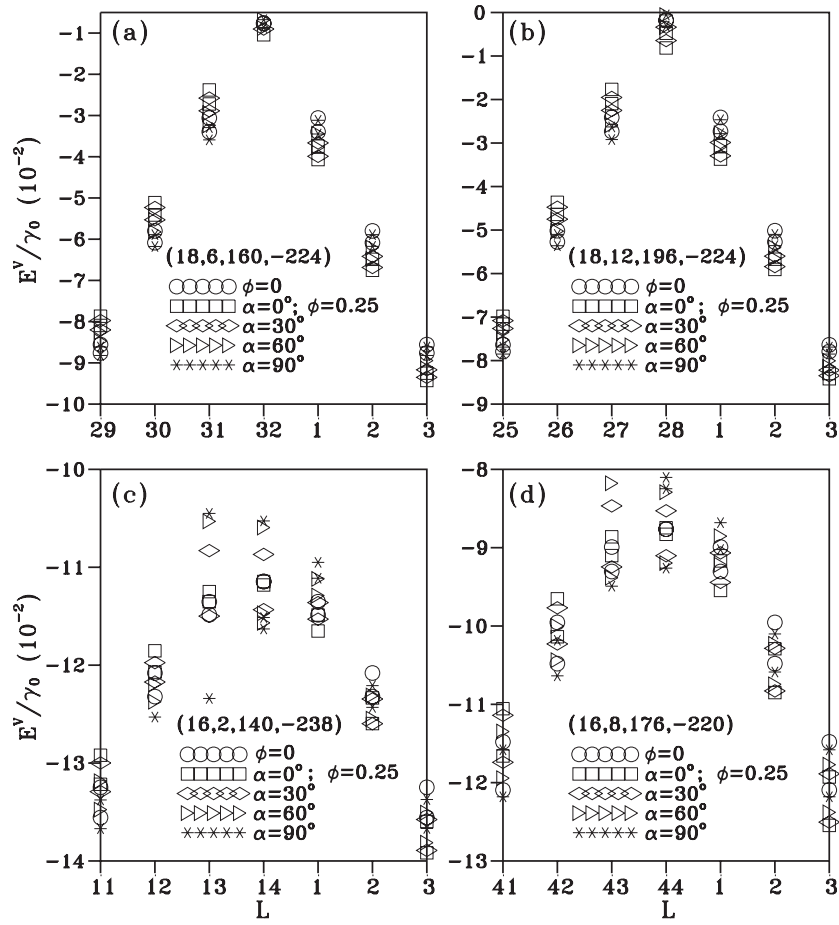
Figure 4. The low-energy magnetoelectronic valence states for the (a) $(18, 6, 160, -224)$, (b) $(18, 12, 196, -224)$, (c) $(16, 2, 140, -238)$, and (d) $(16, 8, 176, -220)$ CCTs at $\phi = 0$, $\phi = 0.25\phi_0$, and different αs.

the magnetic-flux range corresponding to $E_g = 0$ is comparatively narrow. These two results directly reflect the fact that the effect of the parallel magnetic field on the band structure is stronger than that of the perpendicular magnetic field. The ϕ-dependent energy gap strongly relies on the chiral angle, while a simple relation between them is absent. Type-III CCNTs also exhibit similar SMTs, as shown in figures 3(c) and (d). The SMTs occur at $\phi_{\text{SMT}} \sim \phi_0/3$, but not close to zero. Moreover, the gapless magnetic-flux range is much larger than that of type-II CCNTs.

Carbon tori could exhibit a lot of diecrete states, mainly owing to the longitudinal and transverse periodical boundary conditions. The low-energy electronic states of type-II $(18, 6, 160, -224)$ and $(18, 12, 196, -224)$ CCTs are shown in figures 4(a) and (b), respectively. The occupied states are symmetric to the unoccupied states about the Fermi level $E_F = 0$. At $\phi = 0$, each valence (conduction) state is symmetric about the highest occupied state (HOS) (the lowest unoccupied states (LUS)). There is an energy gap between the HOS and the LUS. The energy spacing between states with the same L becomes small as they are gradually away from the HOS. All of the low-energy electronic states are doubly

degenerate. The double degeneracy of the HOS comes from $E(J_l, N_v) = E(J_l', N_v)$, while other degenerate states arise from $E(J_l, L) = E(J_l', N_v - L)$. A simple relation between J_l and J_l' seems to be absent for chiral CTs. Apparently, the HOS, energy spacing, and energy gap strongly depend on chirality.

The effects of a parallel magnetic field on the degenerate state are different, which thus leads to the asymmetry of electronic states about the HOS, the destruction of state degeneracy, the change in the energy gap, and the alternation of the energy spacing. However, the HOS or the LUS stays at the same L. When the magnetic field deviates from the toroid axis, $B_\perp$ induces the coupling of different Ls, in addition to the shift of L from $B_\parallel$. Each state is composed of different Ls. Here it is characterized by a specific L with the maximum probability. At $\phi = 0.25\phi_0$, $B_\perp$ does not alter the principal quantum number of the HOS. Also note that the specific L of the HOS might be changed at large ϕ and $\alpha = 90°$. The state degeneracy at $\alpha = 90°$ is not recovered to the double degeneracy in the $\phi = 0$ case. State energies are lowered or raised with an increase in α, which is dependent on L. The energy spacing is reduced as α increases.

The low-energy magnetoelectronic states of type-III (16, 2, 140, −238) and (16, 8, 176, −220) CCTs are shown in figures 4(c) and (d), respectively. The more complicated coupling effects of Ls from $B_\perp$ result in significant differences between type-III CCTs and type-II CCTs. As to the former: (I) the number of electronic states strongly depends on L as $\alpha > 30°$; (II) the specific L of the HOS might change at $\alpha \geqslant 30°$; (III) the energy spacing exhibits a stronger ϕ-dependence (IV) the energy gap is relativley large; and (V) the energy gap decreases as α grows.

A detailed comparison is made of magnetoelectronic properties between chiral CTs and achiral CTs [41]. The main features of the latter are as follows. In the absence of a magnetic field, the electronic states of armchair $(m, m, p, -p)$ ACTs have double degeneracy $E(J_l, L) = E(m - J_l, N_v - L)$. Those of zigzag $(m, 0, p, -2p)$ ACTs have fourfold degeneracy, except the doubly degenerate HOS or LUS. The fourfold and the double degeneracies come from $E(J_l, L) = (2m - J_l, L) = E(J_l, p - L) = E(2m - J_l, p - L)$ and $E(J_l, p) = E(2m - J_l, p)$, respectively. The magnetic field would destroy the state degeneracy, while armchair ACTs recover double degeneracy at $\alpha = 90°$. As to zigzag ACTs, they exhibit double degeneracy for any α. The specific L of the HOS in armchair ACTs might change at large α and ϕ, and stays unchanged for zigzag ACTs. Armchair ACTs have the smallest energy gaps.

The density of states of type-II CCTs, as shown in figures 5(a) and (b), presents a lot of delta-function-like symmetric peaks due to the quantized discrete states. The height of the peak represents the state degeneracy, and the distance between two neighbouring peaks is the energy spacing between two states. The heights of the prominent peaks in the absence of ϕ correspond to double degeneracy. At $\phi \neq 0$, the destruction of state degeneracy leads to a pair of peak structures without state degeneracy. Their energy spacing would decrease with increasing α. Furthermore, a pair of peaks would approach the Fermi level. There are three main differences between type-II CCTs and type-III CCTs (figures 5(c) and (d)). The latter exhibit the relativley dense peak structures, the smaller energy spacing, and the opposite α-dependence for the energy spacing.

The magnetic-flux-dependent energy gap with the Zeeman splitting is shown at $\phi \leqslant 0.5\phi_0$. At $\alpha = 0°$, E_gs of type-II CCTs exhibit an oscillatory behaviour during the variation of ϕ (figures 6(a) and (b)). E_g reaches its maximum at $\phi = 0.5\phi_0$ and then decreases. The field direction could effectively change the dependence of E_g on ϕ. Such a dependence becomes weak as α increases. This result clearly illustrates that the shift of L ($B_\parallel$) has a stronger effect on the change of state energy, compared with the coupling of Ls ($B_\perp$). Complete energy-gap
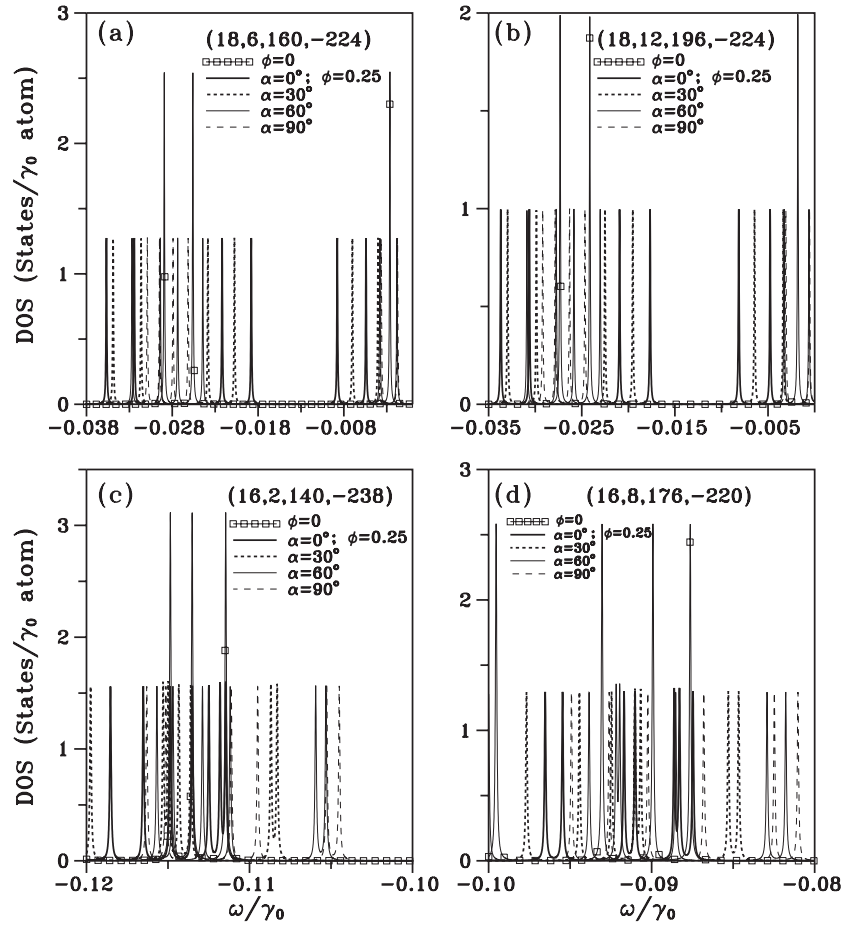
Figure 5. Density of states of the (a) $(18, 6, 160, -224)$, (b) $(18, 12, 196, -224)$, (c) $(16, 2, 140, -238)$, and (d) $(16, 8, 176, -220)$ CCTs at $\phi = 0$; $\phi = 0.25\phi_0$ and different αs.

modulations might happen at large ϕ (not shown). As for type-III CCTs (figures 6(c) and (d)), E_g declines monotonously with increasing ϕ except for the very small AB oscillation about $\phi = 0.5\phi_0$ at $\alpha = 0°$. E_g decreases with an increase in α, and the dependence of E_g on ϕ is relatively strong at large α.

Dimensionalities and geometric structures cause CCTs to differ from CCNTs. These two systems exhibit the delta-function-like peaks and the square-root asymmetric peaks, respectively, in the DOS. The double degeneracy is destroyed at $\alpha = 90°$ for the former, but not for the latter. The dependence of the energy gap on α is opposite for type-III CCTs and CCNTs (figures 3(c), (d), 6(c); (d)). Moreover, complete energy-gap modulations would happen at different ϕ_{SMT}s.

4. Conclusion

In conclusion, we have studied the magnetoelectronic properties of chiral carbon nanotubes and tori using the tight-binding model for any magnetic field. The state energy, density of
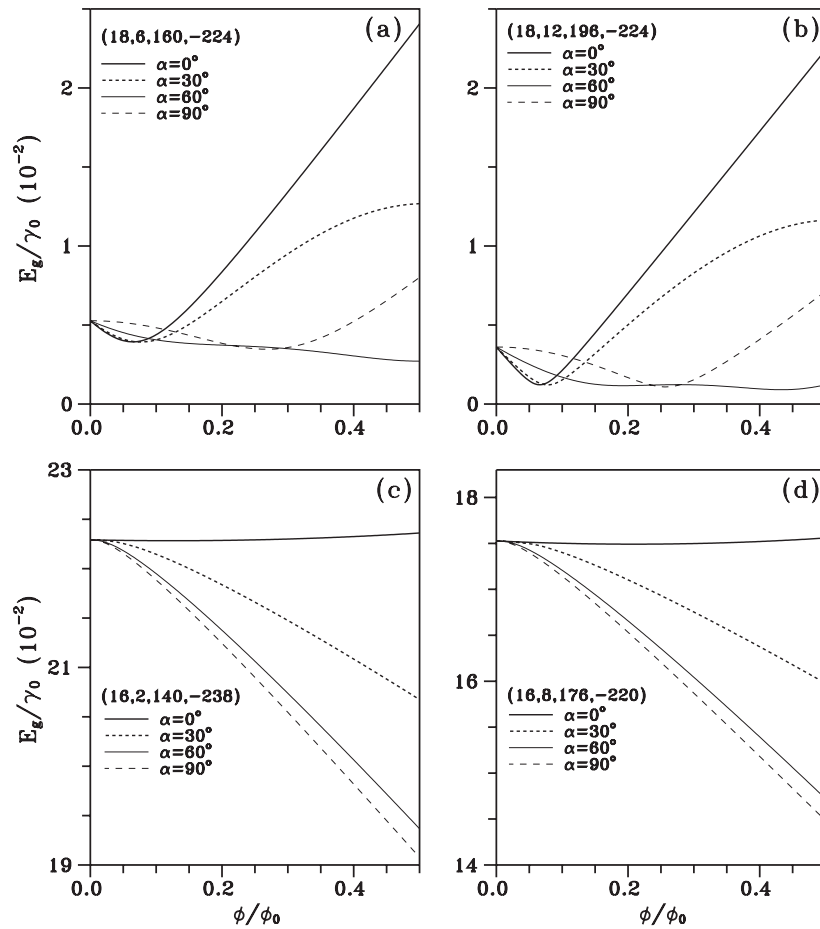
Figure 6. The flux-dependent energy gaps of the (a) $(18, 6, 160, -224)$, (b) $(18, 12, 196, -224)$, (c) $(16, 2, 140, -238)$, and (d) $(16, 8, 176, -220)$ CCTs at different αs.

states, and energy gap strongly depend on the magnitude and direction of the magnetic field, and the chirality. Chiral carbon nanotubes differ quite a lot from achiral carbon nanotubes in band symmetry, band curvature, band crossing, band-edge state, state degeneracy, band spacing, energy gap, and semiconductor–metal transition. For carbon tori, the chirality plays an important role in the number of discrete states of L, the specific L of the HOS, the effects of **B** on energy spacing, the dependence of the energy gap on ϕ and α, and the state degeneracy. The important differences between tori and nanotubes include the energy-gap modulation, the special structures in the density of states, and the state degeneracy. The predicted magnetoelectronic properties could be verified by STM, transport measurements, and absorption spectroscopy.

Acknowledgments

References

[1] Iijima S 1991 *Nature* **354** 56
[2] Mintmire J W, Dunlap B I and White C T 1992 *Phys. Rev. Lett.* **68** 631
[3] Hamada N, Sawada S I and Oshiyama A 1992 *Phys. Rev. Lett.* **68** 1579
[4] Saito R, Fujita M, Dresselhaus G and Dresselhaus M S 1992 *Appl. Phys. Lett.* **60** 2204
[5] Saito R, Fujita M, Dresselhaus G and Dresselhaus M S 1992 *Phys. Rev.* B **46** 1804
[6] Ajiki H and Ando T 1993 *J. Phys. Soc. Japan* **62** 1255
[7] Blase X, Benedict L X, Shirley E L and Louie S G 1994 *Phys. Rev. Lett.* **72** 1878
[8] Kane C K and Mele E J 1997 *Phys. Rev. Lett.* **78** 1932
[9] Shyu F L and Lin M F 2002 *J. Phys. Soc. Japan* **71** 1820
[10] Saito R, Dresselhaus G and Dresselhaus M S 1994 *Phys. Rev.* B **50** 14698
[11] Ajiki H and Ando T 1993 *J. Phys. Soc. Japan* **62** 2470
[12] Ajiki H and Ando T 1995 *J. Phys. Soc. Japan* **64** 260
[13] Ajiki H and Ando T 1996 *J. Phys. Soc. Japan* **65** 505
[14] Lu J P 1995 *Phys. Rev. Lett.* **74** 1123
[15] Shyu F L, Chang C P, Chen R B and Lin M F 2003 *J. Phys. Soc. Japan* **72** 454
[16] Shyu F L, Chang C P, Chen R B, Chiu C W and Lin M F 2003 *Phys. Rev.* B **67** 045405
[17] Chiu C W, Chang C P, Shyu F L, Chen R B and Lin M F 2003 *Phys. Rev.* B **67** 165421
[18] Chiu C W, Shyu F L, Chang C P, Chen R B and Lin M F 2003 *Phys. Lett.* A **311** 63
[19] Wildoer J W G, Venema L C, Rinzler A G, Smalley R E and Dekker C 1998 *Nature* **391** 59
[20] Odom T W, Huang J L, Kim P and Lieber C M 1998 *Nature* **391** 62
[21] Ouyang M, Huang J L, Cheung C L and Lieber C M 2001 *Science* **292** 702
[22] Zhou C, Hong J and Dai H 2000 *Phys. Rev. Lett.* **84** 5604
[23] Fujiwara A, Tomiyama K, Suematsu H, Yamura M and Uchida K 1999 *Phys. Rev.* B **60** 13492
[24] Bachtold A, Strunk C, Salvetat J P, Bonard J M and Forró L 1999 *Nature* **397** 673
[25] Roache S and Saito R 2001 *Phys. Rev. Lett.* **87** 246803
[26] Coskun U C, Wei T C, Vishveshwara S, Goldbart P M and Bezryadin A 2004 *Science* **304** 1132
[27] Liu J, Dai H, Hafner J H, Colbert D T, Smalley R E, Tans S J and Dekker C 1997 *Nature* **385** 780
[28] Martel R, Shea H R and Avouris P 1999 *Nature* **398** 299
[29] Dunlap B I 1992 *Phys. Rev.* B **46** 1933
[30] Itoh S, Ihara S and Kitakami J I 1993 *Phys. Rev.* B **47** 1703
[31] Ihara S, Itoh S and Kitakami J I 1993 *Phys. Rev.* B **47** 12908
[32] Itoh S and Ihara S 1993 *Phys. Rev.* B **48** 8323
[33] Itoh S and Ihara S 1994 *Phys. Rev.* B **49** 13970
[34] Oh D H, Park J M and Kim K S 2000 *Phys. Rev.* B **62** 1600
[35] Ceulemans A, Chibotaru L F and Bovin S A 2000 *J. Chem. Phys.* **112** 4271
[36] Meunier V, Lambin P and Lucas A A 1998 *Phys. Rev.* B **57** 14886
[37] Haddon R C 1997 *Nature* **388** 31
[38] Lin M F, Chen R B and Shyu F L 1998 *Solid State Commun.* **107** 227
[39] Lin M F and Chuu D S 1998 *J. Phys. Soc. Japan* **67** 259
[40] Latgé A, Rocha C G, Wanderley L A L, Pacheco M, Orellana P and Barticevic Z 2003 *Phys. Rev.* B **67** 155413
[41] Shyu F L, Tsai C C, Chang C P, Chen R B and Lin M F 2004 *Carbon* **42** 2879
[42] Tsai C C, Shyu F L, Chiu C W, Chang C P, Chen R B and Lin M F 2004 *Phys. Rev.* B **70** 075411
[43] Lin M F 1998 *J. Phys. Soc. Japan* **67** 2218
[44] Lin M F 1998 *J. Phys. Soc. Japan* **68** 1102